

The 6th International Supercritical CO₂ Power Cycles Symposium
March 27 - 29, 2018, Pittsburgh, Pennsylvania

Investigation of heat transfer model for horizontal tubes at supercritical pressures of CO₂

Tae Ho Kim
Ph.D. Candidate
POSTECH
Pohang-si, Gyeongsangbuk-do
thkim0812@postech.ac.kr

Hyun Sun Park*
Professor
POSTECH
Pohang-si, Gyeongsangbuk-do
hejsunny @postech.ac.kr

Jin Gyu Kwon
Ph.D. Candidate
POSTECH
Pohang-si, Gyeongsangbuk-do
sarahkjg@postech.ac.kr

Joo Hyun Park
Ph.D. Candidate
POSTECH
Pohang-si, Gyeongsangbuk-do
jhpark0425@postech.ac.kr

Moo Hwan Kim
Professor
POSTECH
Pohang-si, Gyeongsangbuk-do
mhkim@postech.ac.kr



Mr. Tae Ho Kim

B.S. Mechanical Engineering, Kyunghee university (13')



Professor. Hyun Sun Park

Ph.D. Nuclear Engineering, Univ. of Wisconsin-Madison ('95)

M.S. Nuclear Engineering, Hanyang university (88')

B.S. Nuclear Engineering, Hanyang university (86')

ABSTRACT

An accurate prediction for heat transfer phenomenon of supercritical CO₂ is one of important issues in order to control a pre-cooler below a pseudocritical temperature. Especially, it is difficult to develop a theoretical or even a semi-empirical heat transfer model in horizontal circular channels due to the buoyancy effect. Buoyancy induced by a drastic density variation of near-wall fluid, causes asymmetric heat transfer coefficients between top and bottom walls. On the other hand, bulk flow acceleration, which occurs in a flow direction by the drastic density variation, causes an identical effect on heat transfer regardless of the flow direction. In this reason, the acceleration effect has been considerably investigated than the buoyancy effect. Therefore, the investigation on the buoyancy effect of horizontal flows should be performed with respect to heat transfer phenomena between the top and bottom walls.

In this study, experiments on heat transfer of supercritical CO₂ were conducted in the horizontal tube having an inner diameter of 7.75 mm. The experimental variables included the inlet temperature, mass flux and heat flux. The tube was electrically heated by the Joule heating method using a DC power supply. The outer wall temperatures were measured by using 10 calibrated K-type thermocouples at the top and bottom walls respectively. From the experimental results, the asymmetric heat transfer coefficients were observed between both walls according to the conditions of mass and heat fluxes. Based on the results, the semi-empirical heat transfer model was obtained by applying a superposition of the forced and natural convections. The model was fitted with our data and compared to other's experimental data. The model showed the reasonable prediction while it should be further analyzed with respect to the valid data.

INTRODUCTION

A Brayton cycle using supercritical CO₂ (SCO₂) as a working fluid has a higher efficiency than the conventional gas Brayton cycle. A high density of SCO₂ near a pseudocritical point enables a compression work to be significantly reduced. The pseudocritical point means the temperature at which a specific heat of the fluid has a maximum value at a constant pressure. The drastic variation of the thermal and hydraulic properties also enables turbomachinery to be miniaturized as well as the compression work reduction. In this point, SCO₂ Brayton cycle can have a compactness and simplicity of the system by using micro or mini channel heat exchangers like PCHE (printed circuit heat exchanger), which has a high thermal efficiency with a large heat transfer area per volume. In these reasons, SCO₂ Brayton cycle has been being developed as a promising power conversion system.

Heat transfer of SCO₂ is an important issue in the SCO₂ power cycle. One of major reasons why the SCO₂ power cycle has the high efficiency is the low compression work due to the high density at the compressor inlet, which adopts the condition slightly below the pseudocritical point. However, the thermal and hydraulic properties vary drastically even when the fluid temperature changes just a little. If the operating condition could not be accurately controlled at the inlet of compressor, the power cycle efficiency would be affected seriously. Therefore, a pre-cooler, which determines the inlet condition of compressor, should be accurately designed and operated. As a result, it is needed to improve the prediction of heat transfer of SCO₂.

Flow acceleration and buoyancy induced by the density variation make a difference between a heat transfer behavior of SCO₂ and that of normal fluids. A large number of researches have been carried out in order to investigate such phenomena on vertical upward and downward flows. Recently, Jackson [1] and Kim and Kim [2-4] developed semi-empirical heat transfer models for the vertical flow based on the shear stress theory in a turbulent boundary layer. In the case of the vertical flow, buoyancy causes the heat transfer deterioration for the upward flow and enhancement for the downward flow while flow acceleration always causes the heat transfer deterioration regardless of the flow direction.

However, in the case of the horizontal flow, the heat transfer characteristics are more complex than that for the vertical flow because buoyancy occurs in a perpendicular direction of the flow. Whiles, flow acceleration still exerts its force in the flow direction. Thus, the turbulence shear stress theory cannot be

applied in terms of buoyancy. For the horizontal flow, buoyancy causes a non-uniform temperature distribution on a circumference. It results in different heat transfer behaviors at the top and bottom sides of the circular tube.

Previous experimental studies investigated the buoyancy effect on heat transfer in horizontal circular channels by using buoyancy parameters. Adebisi and Hall [5] used a criterion in terms of buoyancy parameter Bu_j , defined as $Gr_b Re_b^{-2} (\rho_b / \rho_w) (x/d)^2$. They reported that the buoyancy is negligible when $Bu_j < 10$. Bazargan et al. [6] compared two buoyancy parameters. One is the parameter Bu_c , defined as $Gr_b Re_b^{-2}$. The buoyancy is negligible when $Bu_c < 10^{-3}$ [7]. The other is the parameter Bu_p , defined as $Gr_b Re_b^{-2.75} Pr_b^{-0.5} [1 + 2.4 Re_b^{-1/8} (Pr_b^{2/3} - 1)]^{-1}$. The buoyancy is negligible when $Bu_p < 3 \times 10^{-5}$ [8]. They concluded that the criterion of $Bu_p < 3 \times 10^{-5}$ was more adequate. On the other hand, Yu et al. [9] reported that neither Bu_c nor Bu_p were adequate since both were not able to explain the heat transfer enhancement at the top wall. Recently, Tanimizu and Sadr [10] compared three buoyancy parameters including Bu_c , Bu_j and Bu_p . They concluded that Bu_c showed the best prediction of the buoyancy effect among them. As mentioned above, many researchers reported the contradictory results. In addition, Kim et al. [11] studied such buoyancy parameters in order to determine which parameter is adequate to analyze the buoyancy effect in the horizontal flow. They concluded that the conventional parameters are not adequate since most of the parameters are originated from the buoyancy effect on the vertical flow and the remains was inconsistent with respect to the heat transfer characteristics.

Therefore, a different type of heat transfer model is suggested in this study. Analysis on heat transfer is carried out by introducing a superposition of forced convection and natural convection. In this analysis, the forced convection is affected by only flow acceleration and the natural convection is affected by buoyancy.

EXPERIMENTAL FACILITY [11]

An experimental facility as shown in Fig. 1 was used. The detail description of the facility can be found in our previous study [11]. In this paper, brief explanation of the facility is introduced. The facility consisted of three sections: a CO₂-supplying section, a CO₂-circulation section and a test section. In the CO₂-supplying section, a CO₂ pressure tank fed CO₂ into the circulation system. An air-driven pump (Maximator, G35) with an electric regulator pressurized the circulation loop up to the experimental condition. A magnetic gear pump (Micropump Inc., GC series) circulated CO₂ at a constant motor speed to maintain a constant mass flow rate which was measured by using a coriolis flow meter (RHEONIK, RHM04) with a rated accuracy of 0.20%. Needle valves were used to control the mass flow rate through a bypass line. While passing through the flow meter, CO₂ was heated by a gas circulation heater (WATLOW, Cast-X 2000) with a maximum capacity of 6 kW to increase the inlet temperature of test section up to the experimental condition. The heater was controlled by a power controller (HANYOUNG NUX, TPR-2N) and a temperature controller (Autonics, TZ4ST). Inlet and outlet temperatures of the test section were measured by resistance temperature detectors (RTDs) of 1/10 DIN class that has an accuracy of $\pm 0.07^\circ\text{C}$ at 50°C . Inlet absolute pressure was measured by an absolute pressure transducer (Sungji Tech, PSH) that has an accuracy of $\pm 0.066\%$ in a full-span. After passing through the test section, CO₂ was cooled through a shell-and-tube heat exchanger using water as a coolant supplied by a circulation bath (Lab. Companion, RW-2040G).

The test section shown in Fig. 2 was a circular stainless steel tube with an inner diameter (d) of 7.75 mm. The electrically-heated length (L_h) of the test section was 0.91 m. The entrance length (L_e) of 100 mm ($x/d \approx 13$), which is larger than 10 times of the hydraulic diameter recommended for most of practical turbulent flows in channels, exists before the heated length [12]. Ten K-type thermocouples (TCs) were mechanically fastened at intervals of 8 mm on each of the top and bottom outer walls. All thermocouples were calibrated using the RTD as a reference and had an accuracy of 0.25°C . The experimental data was acquired by a data acquisition system (Agilent, 34980A) when the experimental condition was in a steady

state during 5 minutes. The experiments were sequentially carried out as increasing a heat flux while other variables were controlled at a constant until the cooling capacity was affordable. The experimental conditions are shown in Table 1.

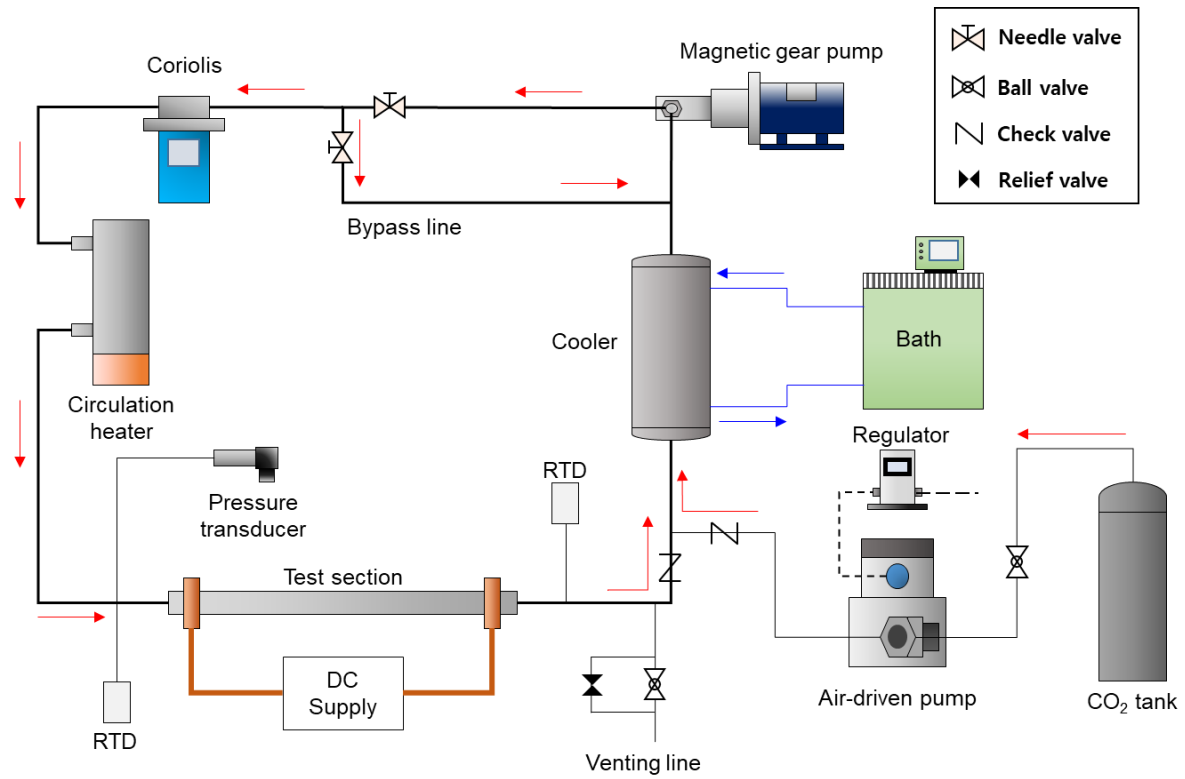


Fig. 1 Schematics of the experimental facility

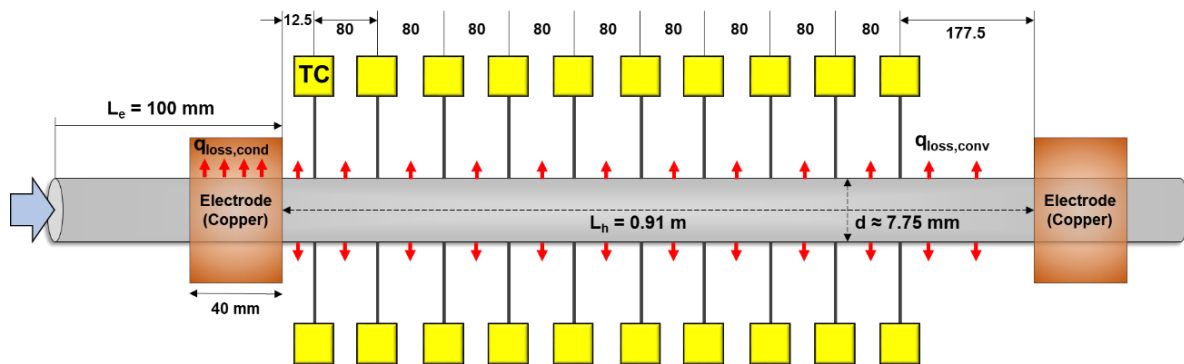


Fig. 2 Schematics of the test section

Table 1 Experimental conditions

Case	P _{in} [bar]	T _{in} [°C]	Re [-]	q [kW/m ²]	G [kg/(m ² ·s)]
T25G60	73.83-74.96	25.02-26.61	6590-7293	1.2-15.5	52.1-60.4
T25G150	75.29-76.28	24.50-25.24	17641-18281	3.4-25.7	147.2-153.2
T25G250	75.02-76.61	24.85-25.18	28639-29605	3.3-29.5	240.2-246.8
T30G070	75.87-76.58	29.72-29.79	9366-10608	3.1-22.1	64.1-73.6
T30G150	76.19-77.26	29.86-30.07	20844-22062	3.1-25.8	143.0-150.8
T30G250	76.22-77.35	29.90-30.00	35216-36817	3.2-25.9	242.9-250.5

DATA REDUCTION [11]

The experimental Nusselt number (Nu_{Exp}) was determined as

$$Nu_{Exp} = \frac{hd}{k_b}, \quad (1)$$

where k_b is the thermal conductivity evaluated at the bulk mean temperature. The local heat transfer coefficient (h) was obtained using the Newton's law of cooling as

$$h = \frac{q}{T_{w,i} - T_b}. \quad (2)$$

In order to calculate the heat transfer coefficient, the heat flux from the inner wall to the fluid, the inner wall temperature and the bulk mean temperature are needed. First, the heat flux is calculated as

$$q = \frac{Q_{PS}}{A_{s,i}} - q_{loss} \frac{D}{d}. \quad (3)$$

In Eq. (3), electric power (Q_{PS}) is calculated as $Q_{PS} = VI$ where "V" means voltage and "I" does current. The inner (d) and outer (D) diameters and the inner wall surface area ($A_{s,i}$) are obtained by geometric information. Then, a heat loss test was carried out to estimate a local heat flux loss. The heat loss test was performed at an atmospheric pressure without a flow inside the tube. In this situation, it is assumed that the power input is totally transferred from the outer wall to the surroundings. Then, the outer wall temperatures for the top and bottom walls ($T_{w,o}$) were measured according to the power input. The surrounding temperature was simultaneously measured since the heat loss depends on the surroundings. The local average temperature of the outer walls ($T_{w,ave}$) was calculated by using the corresponding top and bottom wall temperatures. The local heat flux loss was calculated as the power input over the surface area of the outer wall ($A_{s,o}$). The linear relationship between the local heat flux loss and the temperature difference of the averaged outer wall and the surroundings, i.e. ($T_{w,ave} - T_{surr}$), is shown in Fig. 3. The reason why the temperature measured at the first TC is smaller than other TCs is the heat loss by conduction of the electrode made by copper. Then, the local heat flux loss and constants (a , b) were obtained from the linear relationship expressed as

$$q_{\text{loss}} = a \cdot (T_{w,\text{ave}} - T_{\text{surr}}) + b. \quad (4)$$

Prior to calculate the bulk mean temperature (T_b), the local enthalpy of the bulk mean fluid (i_b) was calculated using the energy balance equation expressed as

$$i_{b,n} = i_{b,n-1} + \left(\frac{q_n + q_{n-1}}{2} \right) [\pi d(x_n - x_{n-1})] / \dot{m}. \quad (5)$$

From the local bulk mean enthalpy and the inlet pressure (P_{in}), the corresponding local bulk mean temperature was calculated using the REFPROP 7.0 software [13], i.e. $T_b = f(i_b, P_{\text{in}})$.

The inner wall temperature ($T_{w,i}$) was calculated using the one-dimensional conduction equation in cylindrical coordinates as

$$T_{w,i} = T_{w,o} - \frac{q_v}{16k} (d^2 - D^2) + \frac{D}{2k} \left(\frac{q_v D}{4} - q_{\text{loss}} \right) \ln \frac{d}{D}, \quad (6)$$

where k means the thermal conductivity of the test section and q_v means the volumetric heat generation. The uniform volumetric heat generation is assumed to the whole test section.

As a correlation for normal heat transfer, which involves “isothermal” properties, the Gnielinski correlation was referred [13]. It is defined as

$$\text{Nu}_{\text{Gn}} = \frac{(f/8)(\text{Re}_b - 1000)\text{Pr}_b}{1 + 12.7(f/8)^{0.5}(\text{Pr}_b^{2/3} - 1)}, \quad (7)$$

in the range of $0.5 \leq \text{Pr}_b \leq 2000$ and $3 \times 10^3 \leq \text{Re}_b \leq 5 \times 10^6$ where $f = [0.79 \ln \text{Re}_b - 1.64]^{-2}$.

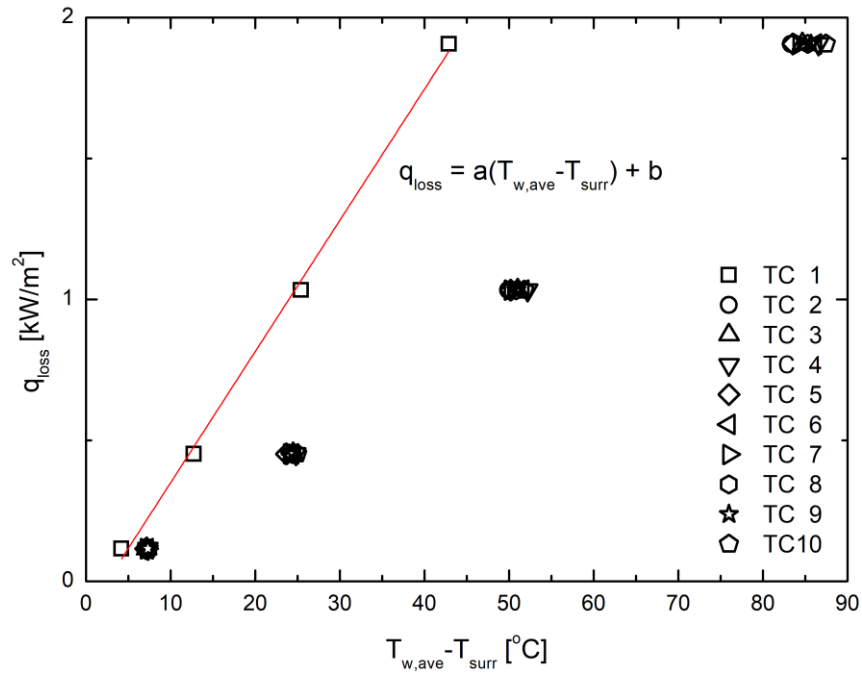


Fig. 3 Local heat flux loss calculation at each TC measuring the wall temperature

UNCERTAINTY ANALYSIS

Experimental data near the pseudocritical temperature has a large uncertainty in spite of using high-accuracy measurement devices. This large discrepancy is originated from a significant change of thermal-hydraulic properties in a very small temperature change. Thus, an uncertainty analysis was performed based on the uncertainty of the measurement. The uncertainty for the Nusselt number can be expressed as

$$\sigma_{Nu}/Nu = \sqrt{\left(\frac{\sigma_h}{h}\right)^2 + \left(\frac{\sigma_{k_b}}{k_b}\right)^2}. \quad (8)$$

In Eq. (8), k_b means the thermal conductivity evaluated at the bulk temperature. The uncertainty for the fluid property was calculated from the maximum and minimum values, which were determined by the accuracy of the temperature and pressure measurements. The uncertainty for the heat transfer coefficient was obtained by

$$\sigma_h/h = \sqrt{\left(\frac{\sigma_q}{q}\right)^2 + \left(\frac{\sigma_{T_{w,i}}}{T_{w,i} - T_b}\right)^2 + \left(\frac{\sigma_{T_b}}{T_{w,i} - T_b}\right)^2}. \quad (9)$$

Now, σ_q and $\sigma_{T_{w,i}}$ were determined by the accuracy of the power supply and the thermocouples. However, σ_{T_b} was calculated with similar to the fluid property since the local bulk temperature was estimated by the enthalpy and the pressure. These were obtained by using Eq. (10)-(12) expressed as

$$\sigma_q = \sqrt{\left(\frac{1}{A_{s,i}} \sigma_{QPS}\right)^2 + \left(\frac{D}{d} \sigma_{q_{loss}}\right)^2}, \quad (10)$$

$$\sigma_{T_{w,i}} = \sqrt{\sigma_{T_{w,o}}^2 + \left\{ \left(\frac{d^2 - D^2}{16k} + \frac{D^2}{8k} \ln \frac{d}{D} \right) \sigma_{qv} \right\}^2 + \left(\frac{D}{2k} \ln \frac{d}{D} \sigma_{q_{loss}} \right)^2}, \quad (11)$$

$$\sigma_{i_{b,n}} = \sqrt{\sigma_{i_{b,n-1}}^2 + \left\{ \frac{\pi d (x_n - x_{n-1})}{2\dot{m}} \right\}^2 (\sigma_{q_n}^2 + \sigma_{q_{n-1}}^2) + \left[\frac{q_n + q_{n-1}}{2} \left\{ \pi d (x_n - x_{n-1}) \right\} \frac{1}{\dot{m}^2} \sigma_{\dot{m}} \right]^2}. \quad (12)$$

The uncertainty of all experimental data for the Nusselt number is indicated in Fig. 4 as a function of a normalized bulk temperature. It is seen that the uncertainty has higher values when the bulk temperature close to the pseudocritical temperature. The maximum uncertainty for each wall is 27.8% for the top wall and 29.6% for the bottom wall.

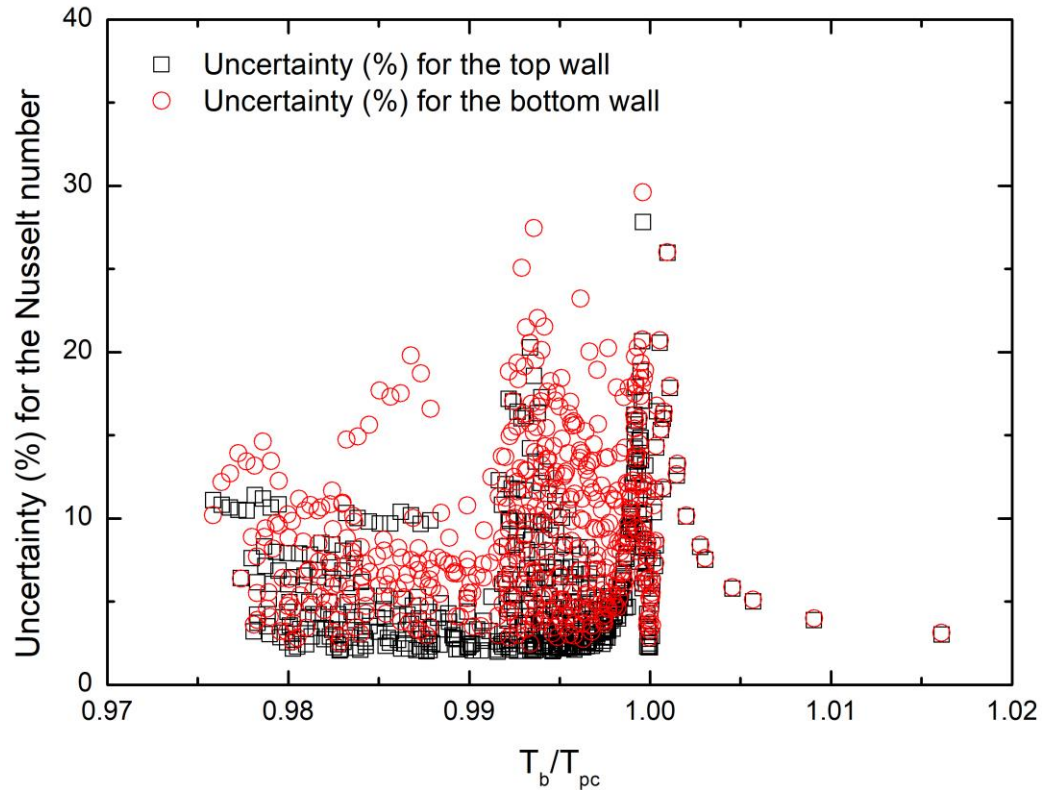


Fig. 4 Uncertainty for the Nusselt number at the top and bottom walls

SEMI-EMPIRICAL HEAT TRANSFER MODEL

Similar characteristics with heat transfer of SCO_2 were reported from studies about heat transfer of air or water in horizontal channels. Osborne and Incropera [14] experimentally studied a mixed convection of water between horizontal and parallel plates. They observed the heat transfer deterioration at the top plate and enhancement at the bottom plate. They explained the heat transfer deterioration with respect to flow acceleration, which induces laminarization, at the top plate and the heat transfer enhancement with respect to buoyancy at the bottom plate. They explained the mixed convection heat transfer by using the superposition of the forced convection and the natural convection in the form of $\text{Nu}_{mc}^n = \text{Nu}_{fc}^n + \text{Nu}_{nc}^n$. In this perspective, heat transfer of SCO_2 in the horizontal tube can be also considered as the superposition of the forced and natural convections. The conceptual idea of the superposition is shown in Fig. 5.

- Forced convection

As studied by many researchers, flow acceleration reduces a shear stress near a wall. Flow acceleration always occurs in a parallel direction of a flow regardless of the orientation. Thus, flow acceleration affects to the forced convection heat transfer in the horizontal tube. Kim and Kim [4] suggested a heat transfer model based on a thermal resistance theory in a turbulent boundary layer divided into a viscous sublayer, a buffer layer and a fully turbulent layer. They approximated the total thermal resistance to the sum of resistance in the viscous sublayer and the buffer layer since the thermal resistance in the fully turbulent layer can be ignored. In this paper, it is assumed that the total thermal resistance can be approximated to the effective boundary layer including the viscous sublayer and some portion of the buffer layer as shown in Fig. 6. The shear stress deformation exists in this effective boundary layer affected by flow acceleration. Then, the total thermal resistance can be expressed as

$$R_{tot} \approx R_{EBL}, \text{ i.e. } \frac{1}{h_{tot}} \approx \frac{1}{h_{EBL}} \text{ or } \frac{1}{Nu_{tot}} \approx \frac{1}{Nu_{EBL}}. \quad (13)$$

In the effective boundary layer, a molecular diffusion is dominant compared to a turbulent diffusion. Thus, heat transfer will be proportional to k_b/δ_{EBL} , that is,

$$h_{EBL} \propto \frac{k}{\delta_{EBL}}. \quad (14)$$

Then, by using the relation of heat transfer coefficient in a dimensionless form, heat transfer affected by flow acceleration over heat transfer by a fluid of isothermal properties can be written as

$$\frac{Nu_{EBL}}{Nu_{iso}} = \frac{\delta_{iso}}{\delta_{EBL}}, \quad (15)$$

where the isothermal properties are identical to the properties at the bulk mean temperature.

Introducing a non-dimensional boundary layer thickness based on the near-wall law, the boundary layer can be expressed as

$$\delta = \left(\frac{\mu}{\sqrt{\rho \tau_w}} \right) \delta^+. \quad (16)$$

Using this expression, the total thermal resistance can be expressed as

$$R_{tot} = \frac{1}{Nu_{EBL}} = \frac{1}{Nu_{iso}} f \left[\left(\frac{\rho_{av}}{\rho_b} \right)^{-0.5}, \left(\frac{\mu_{av}}{\mu_b} \right)^1, \left(\frac{\tau_{w,EBL}}{\tau_{w,iso}} \right)^{-0.5}, \left(\frac{\delta_{EBL}^+}{\delta_{iso}^+} \right)^1 \right], \quad (17)$$

where the subscription ‘‘av’’ means ‘‘integral averaged’’ between the wall and bulk mean temperatures.

From the axial momentum equation in the boundary layer, the shear stress variation is obtained as

$$\Delta \tau_{ac} = \rho_b u_b \frac{du_b}{dx} \delta_{ac}. \quad (18)$$

Applying mass conservation and convection energy conservation equations, $u_b du_b/dx$ is expressed as

$$u_b \frac{du_b}{dx} = \frac{1}{\rho_b c_{p,b} T_b} \frac{4q u_b}{d}. \quad (19)$$

Now, by using the definition of the non-dimensional boundary layer thickness, δ_{ac} can be expressed as

$$\delta_{ac} = \left(\frac{\mu_{av}}{\sqrt{\rho_{av} \tau_{w,iso}}} \right) \delta_{ac}^+. \quad (20)$$

Substituting Eqs. (19) and (20) into Eq. (18), the shear stress variation over the isothermal shear stress is obtained as

$$\frac{\Delta \tau_{ac}}{\tau_{w,iso}} = C \frac{q^+}{Re_b^{-0.625}} \left(\frac{\rho_{av}}{\rho_b} \right)^{-0.5} \left(\frac{\mu_{av}}{\mu_b} \right)^1 \delta_{ac}^+. \quad (21)$$

However, in Eqs. (17) and (20), the non-dimensional boundary layer thicknesses are unknown values since it was not measured in the experiments. While, other variables were obtained from the experiments. Therefore, the constants and indexes obtained from the theoretical method cannot be used since the non-dimensional boundary layer thicknesses might be expressed by other variables. Then, a general form of the equation for the thermal resistance of the effective boundary layer is expressed as

$$\frac{1}{Nu_{EBL}} = \frac{1}{Nu_{iso}} \cdot c_1 Re_b^{n_1} \left(\frac{\rho_{av}}{\rho_b}\right)^{n_2} \left(\frac{\mu_{av}}{\mu_b}\right)^{n_3} (q^+)^{n_4}. \quad (22)$$

where Nu_{iso} is the Nusselt number evaluated at constant properties such as the Dittus-Boelter or the Gnielinski correlation. In this study, Nu_{iso} was selected as the Gnielinski correlation due to the wide applicable range of the Reynolds number.

- Natural convection

Natural convection in enclosures like a circular tube is more complex than that over a flat plate. There are two kinds of natural convection, i.e., “direct” and “indirect” natural convections. The “direct” natural convection means that a buoyant force generates a flow directly, e.g. natural convection on the inclined plate ($0^\circ < \theta < 180^\circ$). On the other hand, the “indirect” natural convection is generated by a pressure drop, i.e., natural convection on the upward facing and downward facing plates ($\theta = 0^\circ, 180^\circ$).

In this reason, it is assumed that a virtual plate, which has a longitudinal length corresponding to the inner diameter of the circular tube, can be considered to be placed at an arbitrary angle of a cross-section of the circular tube. Then, natural convection heat transfer at the arbitrary angle is identical to that of the virtual plate. In this study, the horizontal downward and upward facing plates ($\theta = 0^\circ, 180^\circ$) are considered to the top and bottom walls respectively. For the horizontal plates, a general form of natural convection [15] is expressed as

$$Nu_{nc} = C(Gr_q Pr_b)^n. \quad (23)$$

However, in the case of SCO_2 , the drastic variation of properties should be considered. This can be taken into account by applying the property ratio method [16] to the isothermal correlation. Therefore, a general form of natural convection equation for SCO_2 can be expressed as

$$Nu_{nc} = C(Gr_q Pr_b)^{m_1} \left(\frac{\rho_{av}}{\rho_b}\right)^{m_2} \left(\frac{\mu_{av}}{\mu_b}\right)^{m_3} \left(\frac{\bar{c}_p}{c_{p,b}}\right)^{m_4} \left(\frac{k_{av}}{k_b}\right)^{m_5}. \quad (24)$$

- Mixed convection

As explained, the mixed convection can be regarded as the superposition of forced convection and natural convection. Forced convection affected by flow acceleration will be identical to both top and bottom walls due to symmetry without a gravitational effect. While, natural convection will be different at both walls. Summarizing this, the final forms of the mixed convection equation for each wall are expressed as

$$Nu_{mc,top} = \left\{ [Nu_{fc}]^2 + [Nu_{nc,top}]^2 \right\}^{1/2}$$

$$= \left\{ \left[\frac{1}{Nu_{Gn}} \cdot c_1 Re_b^{n_1} \left(\frac{\rho_{av}}{\rho_b}\right)^{n_2} \left(\frac{\mu_{av}}{\mu_b}\right)^{n_3} (q^+)^{n_4} \right]^{-2} + \left[c_2 (Gr_q Pr_b)^{m_1} \left(\frac{\rho_{av}}{\rho_b}\right)^{m_2} \left(\frac{\mu_{av}}{\mu_b}\right)^{m_3} \left(\frac{\bar{c}_p}{c_{p,b}}\right)^{m_4} \left(\frac{k_{av}}{k_b}\right)^{m_5} \right]^2 \right\}^{1/2} \quad (25)$$

$$Nu_{mc,bot} = \left\{ [Nu_{fc}]^2 + [Nu_{nc,bot}]^2 \right\}^{1/2}$$

$$= \left\{ \left[\frac{1}{Nu_{Gn}} \cdot c_1 Re_b^{n_1} \left(\frac{\rho_{av}}{\rho_b}\right)^{n_2} \left(\frac{\mu_{av}}{\mu_b}\right)^{n_3} (q^+)^{n_4} \right]^{-2} + \left[c_3 (Gr_q Pr_b)^{l_1} \left(\frac{\rho_{av}}{\rho_b}\right)^{l_2} \left(\frac{\mu_{av}}{\mu_b}\right)^{l_3} \left(\frac{\bar{c}_p}{c_{p,b}}\right)^{l_4} \left(\frac{k_{av}}{k_b}\right)^{l_5} \right]^2 \right\}^{1/2} \quad (26)$$

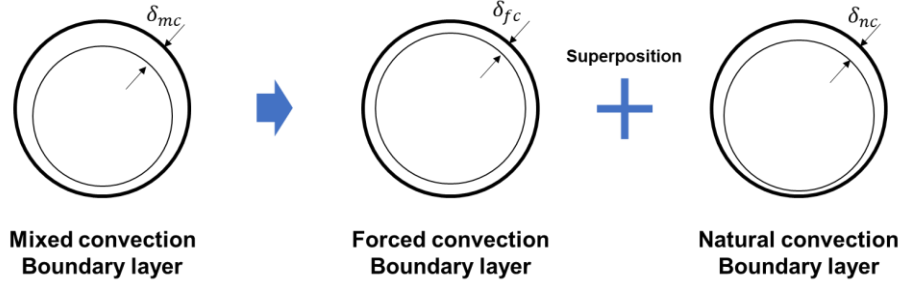


Fig. 5 Concept of a mixed convection boundary layer based on the superposition of the forced and natural convections

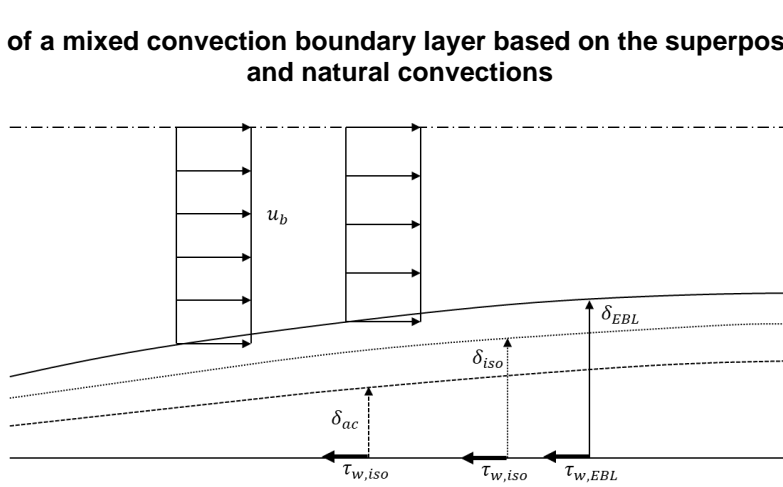


Fig. 6 Concept of a turbulent boundary layer for a forced convection affected by flow acceleration

RESULTS AND DISCUSSION

Mean absolute difference (MAD), mean relative difference (MRD), root mean square deviation (RMSD) and standard deviation (SD) were used to assess the model. Each statistical parameter is defined as

$$\text{MAD} = \frac{1}{n} \sum_{i=1}^n |e_i|, \quad (27)$$

$$\text{MRD} = \frac{1}{n} \sum_{i=1}^n e_i, \quad (28)$$

$$\text{RMSD} = \sqrt{\frac{1}{n} \sum_{i=1}^n e_i^2}, \quad (29)$$

$$\text{SD} = \sqrt{\frac{1}{n-1} \sum_{i=1}^n (e_i - \text{MRD})^2}, \quad (30)$$

where $e_i = (\text{Nu}_{\text{model}} - \text{Nu}_{\text{exp}}) / \text{Nu}_{\text{exp}} \times 100$ and “n” is the total number of data points [17].

All experimental data of our experiments were used to verify the heat transfer model derived in the previous section. Nonlinear fitting function of the Origin software was used in order to find the unknown constants and indexes. To validate our model and the fitted unknown parameters, other’s experimental data were compared with the model. However, the constants (c_1 , c_2 , c_3) were re-fitted to other’s data since the ratio of heat flux to mass flux was different. The selected experimental data was listed in Table 2.

Adebiyi and Hall's data [5] is the cases of the lower ratio of heat flux to mass flux than ours due to the high mass fluxes. While, Tanimizu and Sadr's data [10] is the cases of the higher ratio of heat flux to mass flux than ours due to the high heat fluxes. Figs. 8 and 9 show a comparison of their data with the model fitted by our data. Fig. 9 shows the comparison result only for the top wall since Tanimizu and Sadr [10] reported their data only for the top wall. For each experiment, the constants and indexes are shown in Table 3.

The result is shown in Table 4 and Figs. 7-9. The model has the MADs of 11.37% and 13.20%, the MRDs of 2.37% and 1.79%, the RMSDs of 25.81% and 20.42%, the SDs of 25.72% and 20.36% for the top and bottom walls respectively. The model predicts 472 points (94%) is within an error of $\pm 30\%$ for the top wall and 463 points (92%) is within that of $\pm 30\%$ for the bottom wall among all of 504 data points as shown in Fig. 7.

However, the prediction accuracy was degraded for Adebiyi and Hall's data [5] as it has the MADs of 19.80% and 21.04%, the MRDs of 6.56% and -13.99%, the RMSDs of 25.48% and 25.35%, the SDs of 25.55% and 25.44% for each wall. From the statistics, it is found that the model has over-prediction for the top wall and under-prediction for the bottom wall compared to the average. The RMSDs and SDs were still comparable to our result while that increased for the bottom wall. The model predicts 98 (78%) and 94 (75%) points are within an error of $\pm 30\%$ among 125 data points for each wall as shown in Fig. 8.

The prediction accuracy of the model to Tanimizu and Sadr's data was also degraded as the model has the MAD of 24.57%, the MRD of -0.29%, the RMSD of 34.22% and the SD of 34.33% for the top wall. The model predicts 107 (70%) points are within an error of $\pm 30\%$ among 153 data points as shown in Fig. 9. The model shows neither over-prediction nor under-prediction to the average but the larger RMSD and SD than our result. This also can be seen from Fig. 9. The model has the significant discrepancy for the specific cases.

The reason of the degraded prediction accuracy may result from the different experimental conditions, especially the heat flux and the mass flux. There are two other possible reasons related to the wall and bulk mean temperatures as well as the heat flux to mass flux ratio. When temperature varies at a constant supercritical pressure, the drastic property variation occurs at which the temperature is very close to the pseudocritical temperature. In the case of Adebiyi and Hall's data [5], there are some cases that the wall temperature is lower than the pseudocritical temperature due to the low ratio. However, in the case of Tanimizu and Sadr's data [10], the wall temperature is always higher than the pseudocritical temperature. This can be explained by the bulk mean temperature. Similar to the wall temperature, the significant property variation occurs when the bulk mean temperature is lower than the pseudocritical temperature. Their data includes some cases that the bulk mean temperature is higher than the pseudocritical temperature due to the high ratio.

Nevertheless, the comparison results show the reasonable prediction. It is needed that the wall and bulk mean temperatures are restricted to compare the model more detail in the range that flow acceleration and buoyancy are considered. In addition, a theoretical approach for natural convection should be investigated further as the forced convection was analyzed, since the general form of equation for the natural convection resulted from the empirical method.

Table 2. Experimental conditions of the previous studies

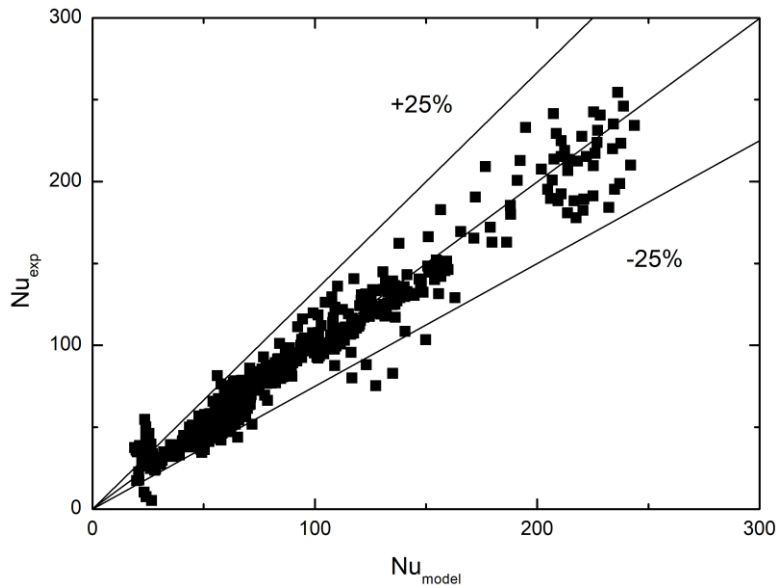
Case	P_{in} [bar]	T_{in} [°C]	Re [-]	q [kW/m ²]	G [kg/(m ² ·s)]
Adebiyi and Hall [5]	75.86-76.14	13.8-30.1	25395-106883	5.1-26.9	104.34-391.91
Tanimizu and Sadr [10]	75-80	24	23915-37686	16-64	185.04-285.97

Table 3. Fitted constants and indexes calculated by using our experimental data

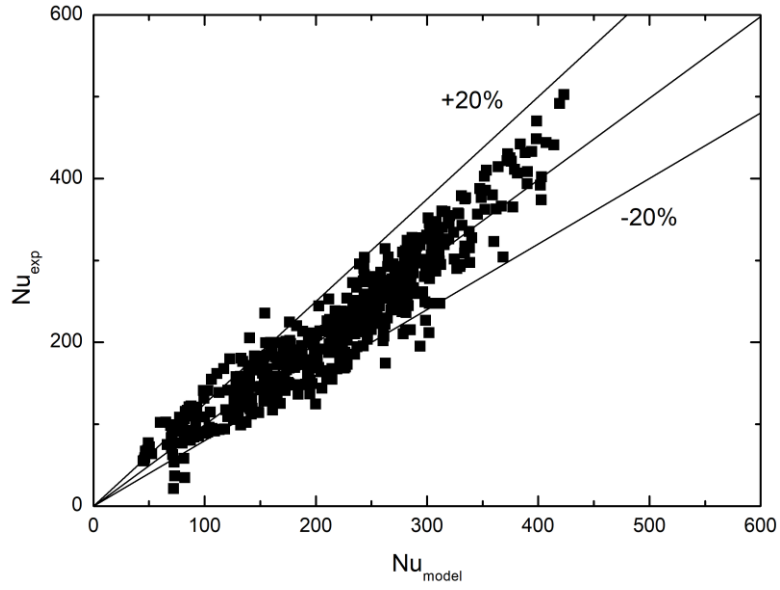
Forced convection		Natural convection (Top wall)		Natural convection (Bottom wall)	
C ₁	1.101e4 (this study)	C ₂	1.603e-2 (this study)	C ₃	2.447e-2 (this study)
	3.268e4 (Adebiyi and Hall)		6.890e-3 (Adebiyi and Hall)		2.294e-2 (Adebiyi and Hall)
	1.030e4 (Tanimizu and Sadr)		1.805e-2 (Tanimizu and Sadr)		-
n ₁	-8.192e-1	m ₁	3.106e-1	l ₁	3.418e-1
n ₂	-5.0	m ₂	1.0e-3	l ₂	1.557
n ₃	4.371	m ₃	-1.982e-1	l ₃	-1.219
n ₄	5.955e-2	m ₄	4.121e-1	l ₄	3.065e-1
-	-	m ₅	-2.031e-1	l ₅	-1.0e-3

Table 4. Statistical assessment of the model for three experiments

Experiment	MAD (%)		MRD (%)		RMSD (%)		SD (%)	
	this study	11.37	13.20	2.37	1.79	25.81	20.42	25.72
Adebiyi and Hall [5]	19.80	21.04	6.56	-13.99	25.48	25.35	25.55	25.44
Tanimizu and Sadr [10]	24.57	-	-0.29	-	34.22	-	34.33	-

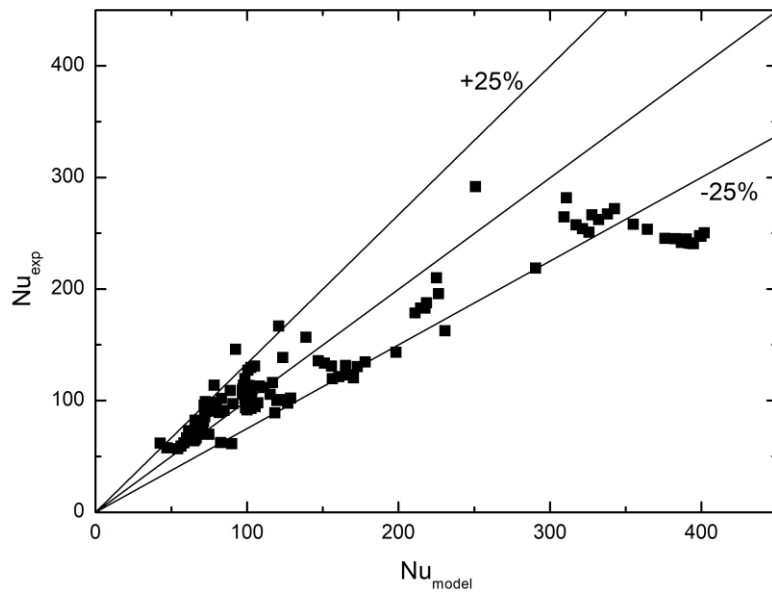


(a) top wall

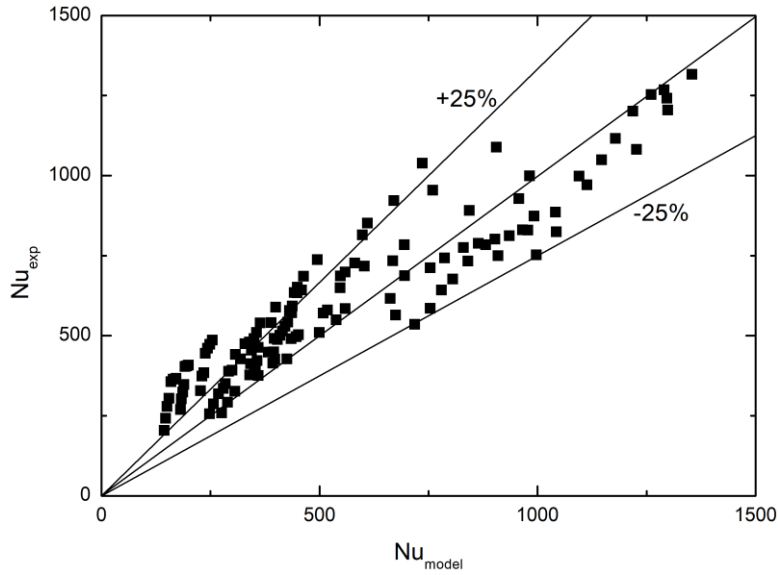


(b) bottom wall

Figure 7. Nonlinear fitting results obtained by using our experimental data



(a) top wall



(b) bottom wall

Figure 8. Comparison between the model and Adebiyi and Hall's data

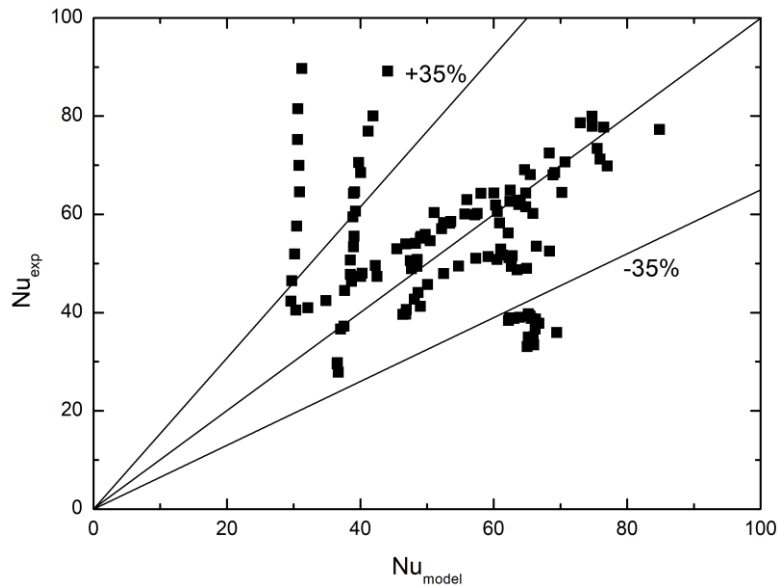


Figure 9. Comparison between the model and Tanimizu and Sadr's data

CONCLUSION

The heat transfer model for the horizontal flow of SCO_2 was suggested based on the superposition of forced convection and natural convection. Forced convection affected by flow acceleration was taken into account by Kim and Kim's model [4] and natural convection affected by buoyancy was done by the empirical form of correlation and the property ratio method. The unknown parameters of the model were fitted by using our experimental data due to the non-dimensional boundary layer thickness. Other

experimental data were compared with the model fitted by ours although the constants were re-fitted with their data. The comparison results were reasonable while the prediction was degraded against our data.

Many correlations have been suggested for supercritical fluids. However, most of the correlations were empirically obtained in the manner of adding the correction factors to the isothermal correlations. The limitation of the empirical correlations is obvious because the correlation suggested by one researcher is not applicable to the result obtained by another researcher. Therefore, it is essential to develop the correlation derived on a theoretical basis although it is not perfectly theoretical.

To identify the model more precisely, the experimental data should be sorted out in the valid conditions where flow acceleration and buoyancy actually occur. The involved conditions may include the wall temperature or the bulk temperature. Furthermore, the theoretical approach is needed to derive the natural convection model as the forced convection was investigated.

REFERENCES

- [1] J. D. Jackson, "Fluid flow and convective heat transfer to fluids at supercritical pressure", *Nuclear Engineering and Design*, 264, pp.24-40, 2013.
- [2] Dong Eok Kim and Moo Hwan Kim, "Experimental study of the effects of flow acceleration and buoyancy on heat transfer in a supercritical fluid flow in a circular tube", *Nuclear Engineering and Design*, 240, pp.3336-3349, 2010.
- [3] Dong Eok Kim and Moo Hwan Kim, "Experimental investigation of heat transfer in vertical upward and downward supercritical CO₂ flow in a circular tube", *Int. J. of Heat and Fluid Flow*, 32, pp.176-191, 2011.
- [4] Dong Eok Kim and Moo Hwan Kim, "Two-layer heat transfer model for supercritical fluid flow in a vertical tube", *J. of Supercritical Fluids*, 58, pp.15-25, 2011.
- [5] G. A. Adebisi and W. B. Hall, "Experimental investigation of heat transfer to supercritical pressure carbon dioxide in a horizontal pipe", *Int. J. Heat Mass Transfer*, Vol. 19, pp.715-720, 1976.
- [6] Majid Bazargan, Daniel Fraser and Vijay Chatoorgan, "Effect of buoyancy on heat transfer in supercritical water flow in a horizontal round tube", *J. of Heat Transfer*, Vol. 127, pp.897-902, 2005.
- [7] S. Kakac, R. K. Shah, W. Aung, Handbook of single-phase convective heat transfer, Wiley, Chap. 18, 1987.
- [8] B. S. Petukhov, A. F. Polyakov, V. A. Kuleshov and Y. L. Sheckter, "Turbulent flow and heat transfer in horizontal tubes with substantial influence of thermo-gravitational forces", *Proc. of 5th Int. Heat Transfer Conference*, Tokyo, Sep. 3-7.
- [9] Shuiqing Yu, Huixiong Li, Xianliang Lei, Yongchang Feng, Yifan Zhang, Hong He and Tai Wang, "Influence of buoyancy on heat transfer to water flowing in horizontal tubes under supercritical pressure", *Applied Thermal Engineering*, 59, pp.380-388, 2013.
- [10] Katsuyoshi Tanimizu and Reza Sadr, "Experimental investigation of buoyancy effects on convection heat transfer of supercritical CO₂ flow in a horizontal tube", *Heat Mass Transfer*, 52, pp.713-726, 2016.
- [11] Tae Ho Kim, Jin Gyu Kwon, Moo Hwan Kim and Hyun Sun Park, "Experimental investigation on validity of buoyancy parameters to heat transfer of CO₂ at supercritical pressures in a horizontal tube", *Experimental Thermal and Fluid Science*, Vol. 92, pp.222-230, 2018.

[12] Yunus A. Cengel and Afshin J. Ghajar, *Heat and Mass Transfer: Fundamentals and Applications*, McGraw-Hill, Fourth Edition, Chap. 8, 2011.

[13] REFPROP software 7.0 version developed by NIST.

[14] D.G. Osborne and F.P. Incropera, "Experimental study of mixed convection heat transfer for transitional and turbulent flow between horizontal, parallel plates", *Int. J. of Heat and Mass Transfer*, Vol. 28, No. 7, pp.1337-1344, 1985.

[15] Tetsu Fujii and Hideaki Imura, "Natural-convection heat transfer from a plate with arbitrary inclination", *Int. J. of Heat and Mass Transfer*, Vol. 15, pp.755-767, 1972.

[16] T.R. Seetharam, K.N. Seetharamu and G.K. Sharma, "Correlations for heat transfer coefficients and wall-temperatures for laminar and turbulent free convection from plane vertical surfaces to supercritical fluids", *Int. J. of Thermal Technologies*, Vol. 6, No. 1, pp.24-31, 2016.

[17] Weiwei Chen, Xiande Fang, Yu Xu and Xianghui Su, "An assessment of correlations of forced convection heat transfer to water at supercritical pressure", *Annals of Nuclear Energy*, 76, pp.451-460, 2015.

ACKNOWLEDGEMENTS

This work was supported by the National Research Foundation of Korea (NRF) grant funded by the Korean government (Ministry of Science and ICT) (No. NRF-2016M2B2B1944981).